A photonic quantum gate based on electrically controlled strong cavity coupling between a single nanocrystal quantum dot and an ultra-high Q silica micro-cavity.

Mark J. Fernée[a], Halina Rubinsztein-Dunlop[a]

[a] Center for Quantum Computer Technology, School of Physical Sciences, The University of Queensland, Queensland, Australia, 4072.

ABSTRACT

We investigate the use of nanocrystal quantum dots as a versatile quantum bus element for preparing various quantum resources for use in photonic quantum technologies. The ability to Stark tune nanocrystal quantum dots allows an important degree of control over the cavity QED interaction. Using this property along with the bi-exciton transition, we demonstrate a photonic CNOT interaction between two logical photonic qubits comprising two cavity field modes each. We find the CNOT interaction to be a robust generator of photonic Bell states, even with relatively large bi-exciton losses.These results are discussed in light of the current state-of-the-art of both microcavity fabrication and recent advances in nanocrystal quantum dot technology. Overall, we find that such a scheme should be feasible in the near future with appropriate refinements to both nanocrystal fabrication technology and micro-cavity design. Such a gate could serve as an active element in photonic-based quantum technologies.

Introduction

All-optical quantum computing is an area of current interest due to the fact that the quantum information carried by photons is extremely robust. This property stems from the fact that photons interact weakly with the environment. A corollary of this is that photons only weakly interact with each other. Thus, it was thought that conditional gate operations with photons would prove to be practically impossible. Surprisingly, Knill et al.[1] discovered that non-deterministic quantum gate operations were actually possible using only simple linear optical elements. Furthermore they showed that it could be possible to build a scalable quantum computer using their architecture. Recent experiments have already demonstrated the basic building blocks for all-optical quantum computing.[2–4]

While all-optical quantum computing has made considerable progress both theoretically and experimentally, it has a number of major hurdles that still must be overcome. The non-deterministic gate operation means that useful quantum circuits suffer dreadful scaling problems, the optical circuitry is still rather large and cumbersome and compact and reliable single photon sources are required.

Many of the hurdles associated with all optical quantum computing could be overcome if the circuitry required to compensate for the non-deterministic nature of the gates could be replaced by a simple deterministic non-linear gate element.[5] Such a gate element would dramatically reduce the overhead required by all-optical quantum computing and potentially allow for miniaturisation of the optical quantum circuits.

A suitable nonlinear gate element could be realised using cavity quantum electrodynamics (CQED) in the strong coupling regime to enhance the non-linear interaction between a single photon and a single quantum object, such as an atom. Various quantum gates have already been demonstrated in the microwave regime and proposed for the optical regime. Furthermore, miniaturisation of CQED schemes has progressed steadily over the last few years. The development of high quality silica micro-tori[6,7] and photonic band-gap structures[8] means that some of the basic building blocks are already in place for producing miniature quantum gates. In particular, miniature fused silica microcavities have already been identified as the most promising candidates for cavity QED in the optical regime.[6,7,9,10]

Further author information: (Send correspondence to M. J. F.)
M. J. F.: E-mail: fernee@physics.uq.edu.au, Telephone: +61 7 3365 3425

Photonics: Design, Technology, and Packaging II, edited by Derek Abbott, Yuri S. Kivshar, Halina H. Rubinsztein-Dunlop, Shanhui Fan, Proc. of SPIE Vol. 6038, 603806, (2006) · 0277-786X/06/$15 · doi: 10.1117/12.651741

However, if we are to pursue miniature quantum gates based on CQED, we need a suitable quantum object. The use of atoms or ions would be ideal if it were possible to trap a single atom/ion and place it into the cavity field. This has already been demonstrated for neutral atoms,[11] but is in practice an extremely difficult task. The main difficulty being that optically active atoms and ions are also extremely chemically active and so have to be carefully isolated from their surroundings.

Alternatively, nanocrystal quantum dots are often referred to as "artificial atoms" and so should also be considered as a suitable quantum object. One main advantage is that while quantum dots are optically active, the ideal quantum dot is not chemically active. Therefore, quantum dots can be incorporated into CQED systems without the need for strong chemical isolation. Furthermore, the position of a quantum dot relative to the cavity field can remain fixed, thus dramatically simplifying the CQED interaction dynamics. Nanocrystal quantum dots coupled to microcavities have already been used to demonstrate single photon sources.[12–15] Quantum gates based on cavity enhanced interactions between quantum dots have been proposed[16] and a quantum gate based on the states within a single quantum dot has already been demonstrated.[17] Therefore it seems that the use of a quantum dot as a quantum object for use in a CQED based quantum gate is worth considering.

In this article we focus on the dc Stark tunability of colloidal quantum dots as a means of providing precise control of the cavity QED interaction. We illustrate the utility of this property by describing an optical CNOT gate that uses a single quantum dot to couple multiple cavity resonances in a fused silica microcavity. We model this gate using a time dependent master equation approach in order to assure that system losses are accounted for. The parameters for the model are drawn from known properties of state-of-the-art colloidal nanocrystal and high Q micro-cavity research.. We discuss the results in light of the known properties of the various physical elements.

Gate operation principle

We investigate the use of the exciton transition in quantum dots to transfer quantum information and the bi-exciton transition to introduce a conditional phase shift, in direct analogy with the phase gate already demonstrated in microwave CQED.[18] This is accomplished by using Stark tuning the exciton and bi-exciton transitions into and out of resonance with a microcavity field mode. It is useful that the bi-exciton energy shift is quite small, so that both the exciton and bi-exciton resonance can be Stark tuned to the same cavity mode, which is necessary for both state preparation and gate operation. The bi-exciton shift in CdSe nanocrystals is of the order of 10 meV, which is well within the 35 meV Stark tunable range of a CdSe nanocrystal that has been previously reported.[19] The implementation of a CNOT gate based on a 3-level "atom" means that the entire gate sequence can be accomplished rapidly using Stark shifting pulses and vacuum Rabi cycling.

The exact form of the micro-cavity may range from micro-spheres to micro-toroids, the important factor being the presence of sufficient high-Q cavity modes in a reasonably small spectral range. We will return to this requirement later, but for now assume that nanocrystal can be brought into resonance with at least four high Q field modes using the dc Stark effect.[19]

In contrast to the gate demonstrated in microwave cavity QED,[18] the "atom" in our gate travels through frequency space, and thus can remain fixed in real space. The proposed physical gate is depicted in Figure 1a, consisting of a single nanocrystal quantum dot placed on the surface of a high Q/V fused silica micro-cavity (a toroidal cavity is depicted) with a fibre taper to couple out the cavity modes to a detector. Electrodes are placed nearby to allow Stark tuning of the nanocrystal resonance and a laser is used to excite the nanocrystal in order to initialise the states of the system. The use of the bi-exciton transition to implement a conditional phase gate that forms the basis of the CNOT gate, is illustrated in figure 1a. The quantum state can be a superposition between the ground and the single exciton state $|X\rangle$, which is depicted in the diagram by thick lines. The single exciton state is subject to a phase shift if and only if there is a photon in the control mode resonant with the bi-exciton transition. The bi-exciton state $|XX\rangle$ is indicated by a dashed line in order to show that it is only transiently populated during the gate operation. This mode of operation does require the splitting of the spin degeneracy of the exciton state. This can be accomplished with an applied magnetic field.[20]

The all-optical or photonic CNOT gate thus uses the field-atom conditional phase shift interaction. However both prior to and immediately following the phase gate interaction, the quantum information is stored solely in

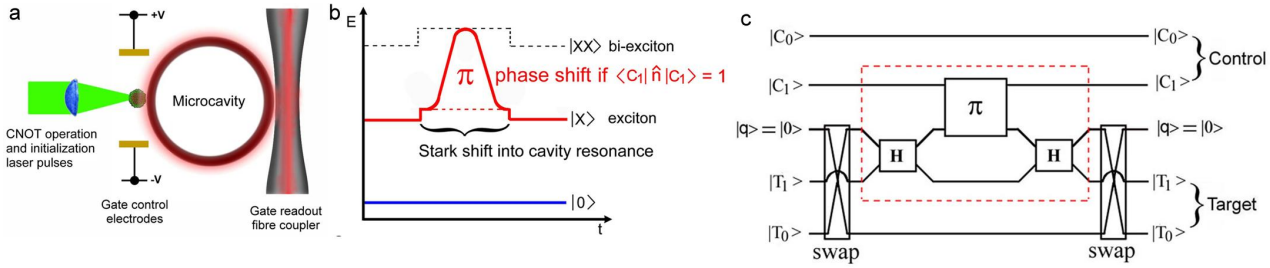

Figure 1.

a) Schematic of a proposed experimental implementation. A single nanocrystal quantum dot sits on the surface of a toroidal microcavity. Laser pulses are used for both initial state preparation and the CNOT operation. Electrodes are used for Stark tuning the quantum dot between the different cavity resonances. A fibre taper is used to couple the field modes to the detection system. b) The three levels of the quantum dot system. Both the ground state, $|0\rangle$ and the exciton state, $|X\rangle$ can be occupied in any superposition state and so are illustrated using thick coloured lines. The bi-exciton state, $|XX\rangle$ does not contain any quantum information, so is unoccupied during most of the gate operation and si is represented by a dashed line. The Stark tuning of the biexciton transition into resonance with the control qubit $|1\rangle$ state cavity mode is illustrated. Transient occupation of the bi-exciton level is only possible if there is a photon in the cavity mode. c) A diagram representing all relevant quantum objects involved in the photonic CNOT gate. Four field modes, comprising the two logical qubits as well as the quantum dot state are indicated. Only single photon occupancy is permitted in the computational basis. The quantum dot acts solely as a quantum bus. Therefore the first operation is a swap gate that loads the information in the target qubit $|0\rangle$ state into the quantum dot. A Hadamard gate is then implemented between the quantum dot and the target qubit $|1\rangle$ state. The quantum dot then undergoes a conditional phase shift and the sequence is reversed, leaving all the quantum information in the photonic qubits and the quantum dot in the ground state. The red dashed line represents the part of the photonic CNOT gate that is simulated. The swap gates are simulated separately.

the optical field modes. Thus the atom (quantum dot) is used to read and manipulate the quantum information contained in the field modes. A schematic for a 4-mode all-optical CNOT gate is presented in figure 1c. Here the quantum information is represented in a logical qubit basis comprising two field modes to represent a single qubit. Therefore, a requirement of the quantum dot is that the excitonic resonance can be Stark tuned across all four cavity modes, while the bi-excitonic resonance can be tuned into resonance with the field mode representing the control qubit in the $|1\rangle$ state. Such a logical qubit system has the advantage that atomic losses result in states that exist outside the computational basis and hence are easily detected. This is especially useful for detecting Auger ionisation losses from the bi-exciton state.

The use of a logical computational basis has many benefits for experimental implementation. The use of two field modes per qubit means that arbitrary superposition states can be prepared from a single quantum dot excitation, by a process of vacuum Rabi cycling that transfers a fraction of the excitation to one mode and the remainder to the other. This allows a quantum state to be rapidly prepared in a time far shorter than the lifetime of the quantum dot excited state. Two successive excitations of the quantum dot can therefore be used to rapidly prepare the initial 2 qubit quantum state of the CNOT system. The other major benefit is that the use of a logical basis can ensure that certain system losses are readily detected and can be corrected by re-running the gate. Therefore, the statistics of gate operation can be obtained only from operations where two quanta are detected in the appropriate modes. These types of quantum schemes form excellent test beds for quantum gates, as they allow for the use of inefficient detection systems.[2]

Cavity QED parameters with quantum dots

There are a number of factors that must be carefully considered if we are going to estimate the optimal coupling strength of a cavity/quantum dot system. The optimisation of microcavities for cavity QED has been carefully considered by Buck and Kimble for fused silica microspheres,[10] and Spillane et. al for fused silica micro-toroids.[7] In both cases the calculation were aimed at optimising the cavities for use with the D_2 transition in Cesium.

A number of parameters are necessary to characterise a cavity QED interaction. For the atom we must know both the excited state decay rate, $1/T_1$, the dephasing rate, $1/T_2$ and the emission wavelength λ_a. For the cavity, we must know the cavity decay rate, κ and the mode volume V_{mode}. The coupling strength can then be defined as follows,

$$g = D\sqrt{\frac{\hbar\omega_a}{2\varepsilon V_{\mathrm{mode}}}}, \tag{1}$$

where D is the emission dipole matrix element. For cavity QED it is simpler to express the coupling constant in terms of the spontaneous emission decay rate, $\gamma_\perp = 1/T_1$ as follows,

$$g = \gamma_\perp \left|\Phi_{\mathrm{surf}}/\Phi_{\mathrm{max}}\right| \sqrt{\frac{V_0}{V_{\mathrm{mode}}}}, \tag{2}$$

where $|\Phi_{\mathrm{surf}}/\Phi_{\mathrm{max}}|$ is the normalized electric field amplitude at the surface of the microcavity and

$$V_0 = \frac{3c\lambda_a^2}{4\pi\gamma_\perp} \tag{3}$$

is the atomic mode volume and $\gamma_\perp$ is the transverse decay rate.

This latter definition of the coupling strength g allows us to readily calculate the cavity QED coupling parameter for different quantum dots by comparing with the results obtained for the Cesium D_2 transition.

For operation in the strong coupling regime, we require the coupling parameter, $g >> 1/T_2, \kappa$. For optimal operation, neither the cavity nor atom dominates the losses in the coupled system. Therefore we define a strong coupling figure of merit, $M = g/\max(\kappa, \gamma)$, where γ is the linewidth of the atomic transition, which is either given by the greater of $1/T_1$ and $1/T_2$. The figure of merit effectively counts the number of Rabi oscillations before the system decoheres and as such is the most useful measure for this discussion.

First we summarise the results obtained for the Cesium D_2 transition at 852.359 nm for both a physically realised system and near the ultimate limit of the technology for both fused silica microspheres and microtoroids. The Cesium D_2 transition has a transverse spontaneous decay rate, $\gamma_\perp$ of 2.61 MHz.
(A): For an experimantally realised microsphere of radius $r = 10\,\mu$m, with a Q of 0.8×10^7 and mode volume of $140\,\mu\mathrm{m}^3$, the coupling strength is $g = 233$ MHz and M = 90.
(B): For a state-of-the-art microsphere of radius $r = 7.83\,\mu$m, with a Q of 9.76×10^8 and mode volume of $90\,\mu\mathrm{m}^3$, the coupling strength is $g = 318$ MHz and M = 120.
(C): For an experimentally realised microtoroid with a principal diameter $D = 50\,\mu$m, a minor diameter $d = 6\,\mu$m, a Q of 1.2×10^8 and mode volume of $1030\,\mu\mathrm{m}^3$, $g = 86$ MHz and M = 30.
(D): For a state-of-the-art microtoroid with a principal diameter $D = 13\,\mu$m, a minor diameter $d = 3.5\,\mu$m, a Q of 1.8×10^8 and mode volume of $37.5\,\mu\mathrm{m}^3$, $g = 450$ MHz and M = 172.

The lead chalcogenide nanocrystal quantum dots are interesting candidates for operation in the strong cavity coupling regime. These binary semiconductors have a highly symmetric rocksalt crystal structure, which is uncommon amongst the wide variety of nanocrystal materials. This results in highly symmetric electron and hole bands where the valence band doesn't split into a combination of heavy and light holes.[21] Therefore conduction-valence band mixing is not predicted to produce any dark states.[21–24] Furthermore, the high dielectric constants of the lead chalcogenides can result in dielectric screening of the transition dipole moment.[22,25] This results in optical transitions with extremely long lifetimes of the order of microseconds.[22,26] In the absence of any other dephasing mechanism, these quantum dots present an almost ideal system for use with fused silica microcavities,

as $\gamma_\perp \approx \kappa$ is possible, which would correspond to minimising both the critical atom number and critical photon number in this system.[10]

We consider PbS nanocrystals, which can exhibit sufficient quantum confinement to blueshift of the band-edge exciton emission to 850 nm. For an exciton lifetime of 500 ns we would obtain the following,
(A): $g = 81$ MHz and M = 1.8,
(B): $g = 111$ MHz and M = 307,
(C): $g = 30$ MHz and M = 10,
(D): $g = 157$ MHz and M = 80,

The estimations above suggest that it may be possible to extend far into the strong coupling regime (eg. M = 307) with such nanocrystals. It is also clear that for such a material, the micro-resonator must possess a Q near the best that can be obtained, while minimising the mode volume is less critical. In fact the numbers presented above are slightly misleading, as they are obtained from optimisations of the CQED sytem for operation with Cesium atoms (cases (B) and (D)). Therefore, it is likely that the micro-toroids will perform better than the microspheres when optimised for the nanocrystal quantum dot in question due to the advantage of being able to quasi-independently adjust both the cavity Q and mode volume.[7] Furthermore, the estimations suggest that operation in the strong coupling regime would be possible with both the current state-of-the-art in both microsphere and microtoroid resonators.

It is the figure of merit that best defines the simulation regime. The challenge is to then choose a value for M that gives both good results for the simulated gate operation, but is also experimentally achievable using current or projected technology. We have chosen a value of M = 100, which could be achieved with the current technology.

The above figure of merit applies to the excitonic transition. For the bi-esxcitonic transition, this figure of merit is far less probable due to the increasing loss due to Auger ionisation. Therefore, we have considered a range of possible biexciton linewidths that correspond to g_{XX}/κ_{XX} ratios from 1 to 100. As there is only transient population of the bi-exciton state, lower figures of merit can be tolerated for this transition.

Stark tuning the nanocrystal

The central idea in our proposed gate is to tune the nanocrystal excited state energy using the dc Stark effect. This can allow frequency tuning across a wide spectral range, depending on the polarizability of the excitonic state. The polarisability of many of the available nanocrystals is not well known. However, most nanocrystal quantum dots display spectral diffusion, which is an indicator of strong polarizability. In particular, the polarizability of CdSe nanocrystals has been thoroughly studied. Stark tuning of the nanocrystal resonance across more than 10 THz was demonstrated.[19] In practice, Stark tuning would need to be restricted to a few GHz in order to prevent the qubits having excessively rapid rotating phases. Aside from CdSe, larger nanocrystals would be expected to have a reasonable polarizability due to weaker quantum confinement, while smaller nanocrystals displaying strong quantum confinement should be less polarizable. Therefore it may be possible to choose an appropriate polarizability based on either the quantum dot material or size. In fact a smaller polarizability may be desirable in order to suppress excess noise from spurious or fluctuating fields.

Initial state preparation

The most direct means of preparing an initial photonic qubit in the logical basis is by first exciting the nanocrystal in order to produce an exciton pair (which recombines with the emission of a photon). Excitation of the nanocrystal may be done by a number of ways, the most direct being via optical absorption. The excited nanocrystal is then rapidly Stark tuned into resonance with the first cavity mode, representing either the logical $|0\rangle$ or logical $|1\rangle$ state and is left to Rabi cycle for some pre-determined time. The Rabi cycling is ended, by rapidly tuning the nanocrystal out of resonance, when the required probability amplitude for the state is reached. The nanocrystal is then Stark tuned into resonance with the second mode comprising the logical qubit and is left to Rabi cycle for exactly half a cycle, so that the remainder of the probability amplitude is transferred into the field mode. This also leaves the nanocrystal in the unexcited state, allowing it to be used to either prepare

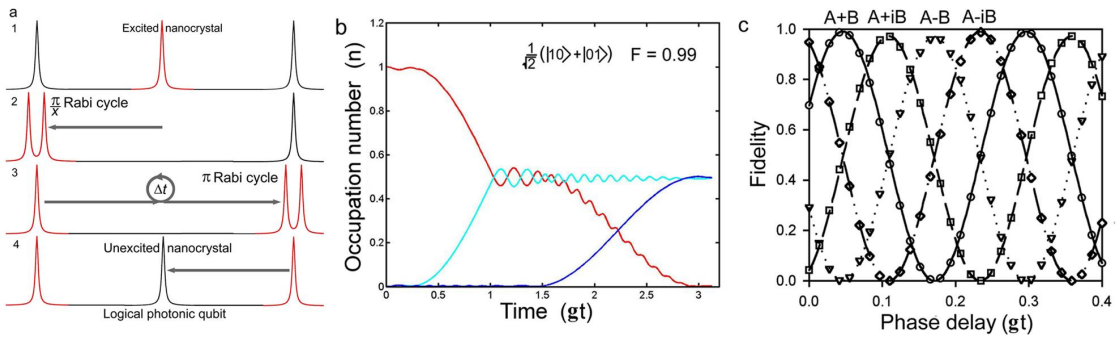

Figure 2.

a) An illustration of the logical qubit initialization sequence. The peaks represent two field modes of the microcavity system (on each end) and the nanocrystal resonance (in the centre). Step 1 the nanocrystal is promoted to its excited state. Step 2, the nanocrystal is rapidly Stark tuned on to resonance with the left cavity mode for a time corresponding to a pre-determined fraction of a Rabi cycle. Step 3 the nanocrystal is rapidly Stark tuned on to resonance with the right cavity mode. A certain delay, Δt, is introduced to adjust the phase of the qubit. The nanocrystal is left on resonance for a time sufficient to accomplish a π Rabi cycle. Step 4 the now unexcited nanocrystal is rapidly Stark tuned away from the cavity mode resonances leaving the two cavity modes in a known superposition state of zero and one photon (a logical qubit). b) The simulated output for the logical qubit initialization sequence (including the maximum fidelity that can be achieved for creating the symmetric superposition state). c) The fidelity plotted as a function of the delay time for creating either of four superposition states that vary only in their phase (by steps of $\pi/2$), indicating that any point on the Bloch sphere can be reached.

another logical qubit or be used in the CNOT gate. Phase rotations around the Bloch sphere are achieved by adjusting the time, Δt, between the two Rabi interactions. The initialisation sequence is illustrated in figure 2a. A simulation of the preparation of the symmetric superposition state $\sqrt{\frac{1}{2}}(|10\rangle + |01\rangle)$ is shown in figure 2b, which can be accomplished with a fidelity of 0.99. The timing delays required to adjust the phase of the superposition is shown in figure 2c. Here we have plotted the fidelities of obtaining either the symmetric, anti-symmetric or the two quadrature superposition states. The oscillations provide an indication that the phase of the state is uniformly rotating around the Bloch sphere. These simulations indicate that arbitrary initial states in a logical qubit basis can be created with high fidelity from a single nanocrystal excitation.

Simulation of the CNOT interaction

Simulations of the field-atom system were carried out using two field modes and a 3-level atomic system, comprising the subsystem indicated in the dashed box in figure 1c. One of the field modes represents the control qubit in the state $|1\rangle$, while the other field mode represents the target qubit in the state $|1\rangle$. The remainder of the target qubit (ie. the amplitude of the target state $|0\rangle$) is assumed to be already transferred to the quantum dot exciton state.

For the simulation we express the generalized 3-level system in terms of exciton and bi-exciton Pauli operators, which in some sense is more satisfying for the quantum dot system. The Hamiltonian is shown below, where we have used an energy offset relative to the control qubit mode,

$$\begin{aligned} \hat{H}/\hbar &= \Delta_m \, \hat{a}_T^\dagger \hat{a}_T + \Delta_X \, \hat{\sigma}_+^X \hat{\sigma}_-^X + \Delta_{XX} \, \hat{\sigma}_+^{XX} \hat{\sigma}_-^{XX} \\ &\quad + i g_X \sum_{i=C,T} \left(\hat{a}_i \hat{\sigma}_+^X - \hat{a}_i^\dagger \hat{\sigma}_-^X \right) \end{aligned}$$

$$+ig_{XX}\sum_{i=C,T}\left(\hat{a}_i\hat{\sigma}_+^{XX}-\hat{a}_i^\dagger\hat{\sigma}_-^{XX}\right)\hat{\sigma}_+^X\hat{\sigma}_-^X$$
$$+A(t)\left(\hat{\sigma}_+^X\hat{\sigma}_-^X+\hat{\sigma}_+^{XX}\hat{\sigma}_-^{XX}\right) \quad (4)$$

The constants Δ_m, Δ_X and Δ_{XX} correspond to the mode separation and the frequency offsets of the quantum dot excitonic and bi-excitonic transitions respectively. The time dependent Stark shifting term, $A(t)$ represents a sequence of Stark shifting pulses. The first pulse is used to perform a Hadamard gate between the quantum dot exciton state and the target qubit cavity mode. The quantum dot is then Stark tuned so that the bi-exciton transition is resonant with the control qubit field mode for a time sufficient to cause a complete Rabi cycle and a π phase shift. The quantum dot is then Stark tuned back into resonance with the target qubit cavity mode where another Hadamard gate is performed between the quantum dot exciton state and the target qubit cavity mode. This subset of the entire gate operation sequence was chosen in order to minimise the effective Hilbert space required for the simulation. The extra swap gates that are used in the entire gate sequence have been simulated separately.

In order to simulate actual gate operation, we include loss terms using the master equation in standard Linblad form. In this case, the master equation is simply represented as follows,

$$L=\frac{1}{i}\left[\hat{H},\rho\right]+\sum_{l=1}^{4}C_l\hat{\rho}\,C_l^\dagger-\frac{1}{2}\left(C_l^\dagger C_l\,\hat{\rho}+\hat{\rho}\,C_l^\dagger C_l\right) \quad (5)$$

Where the loss terms, $C_1=\sqrt{\kappa}\,\hat{a}_T$, $C_2=\sqrt{\kappa}\,\hat{a}_C$, $C_3=\sqrt{\gamma_X}\,\hat{\sigma}_-^X$ and $C_4=\sqrt{\gamma_{XX}}\,\hat{\sigma}_-^{XX}$ represent the coupling of both the target and control cavity modes to other modes outside the cavity, and the spontaneous emission from both the exciton and bi-exciton states respectively, with γ_X and γ_{XX} being the spontaneous emission decay rate of the exciton and bi-exciton states and κ is the cavity decay rate for both field modes.

We numerically integrate the master equation in order to simulate the gate operation. Using the Stark pulse sequence illustrated in figure 3, we simulate all the states represented in the CNOT truth table. The results presented in figure 4 represent the populations of the two field modes and the atom during the course of the interaction. The fidelity of the gate operation is also included. These simulations represent the case where the spontaneous emission loss of the bi-exciton state is equal to that of the exciton state, with a $\gamma_{XX}/g_{XX}=0.01$. This is the low loss case and is simply used to illustrate the CNOT interaction.

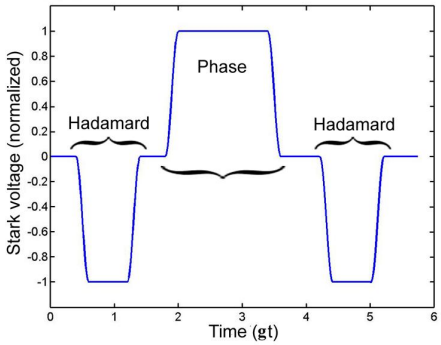

Figure 3.
The Stark shift pulse sequence used to implement a CNOT interaction between two field modes The initial and final Hadamard pulses are used to Stark shift the exciton state into resonance with the target $|1\rangle$ state to initiate Rabi cycling between the nanocrystal and cavity mode . A $\pi/2$ Rabi cycle is applied in each case. The phase gate is implemented by Stark shifting the bi-exciton transition into resonance with the control quibit $|1\rangle$ state. A 2π Rabi cycle is applied in order to generate a π phase shift of the exciton state $|X\rangle$.

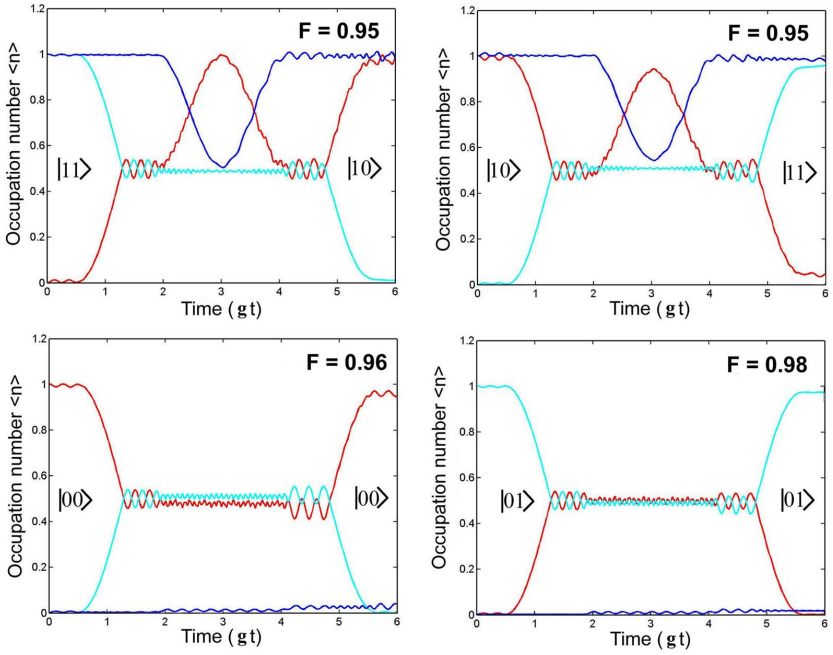

Figure 4.
A series of simulated CNOT interactions for the bi-excitonic gate representing the CNOT truth table. The occupation number of the quantum dot represents a sum of the occupation numbers for the exciton state and the bi-exciton state. Input and output states are indicated and the gate fidelity is also given. $g_x/\gamma_x = g_{xx}/\gamma_{xx} = 100$ are used for thes simulations in order to demonstrate the basic CNOT interaction.

The ultimate test of the CNOT interaction is its ability to generate entangled or Bell states. We have also run the simulation for a range of γ_{xx}/g_{xx} values, inorder to estimate the effect of biexciton loss on the gate operation. The fidelities of Bell state formation are included in table 1 below.

Table 1. Fidelity for generation of Bell states

Bell State	0.01	0.1	0.2	0.5	1
$\|10\rangle + \|01\rangle$	0.97	0.96	0.95	0.91	0.86
$\|10\rangle - \|01\rangle$	0.97	0.96	0.95	0.91	0.86
$\|11\rangle + \|00\rangle$	0.94	0.93	0.92	0.88	0.84
$\|11\rangle - \|00\rangle$	0.94	0.93	0.92	0.88	0.84

Discussion

In general, the operation of the photonic CNOT gate based around a conditional phase shift using the bi-exciton transition in quantum dots seems to yield very high fidelities. Furthermore, the operation is not highly sensitive to bi-exciton losses. In fact this photonic gate is able to detect all quantum dot losses, as such losses will take the system out of the computational basis. Therefore, operation of the quantum dot based CNOT gate using correlated photon counting should in principle detect many loss-based errors, enabling the gate to be effectively run with much higher fidelity.

Experimental implementation of the proposed photonic CNOT gate relies primarily on the material properties

of the gate's constituents. Recent advances in the fabrication of fused silica microcavities have shown that these devices have the potential to facilitate CQED interactions well into the strong cavity-coupling regime.[7,10] The main points that need to be addressed are the fabrication of a microcavity with an appropriate mode structure and also the use of a nanocrystal quantum dot with an appropriate lifetime and with decoherence properties approaching the lifetime limit. A suitable mode structure will probably involve transverse mode engineering. For example transverse modes in microspheres can have a reasonable mode separation, which should be sufficient for the task.[27] The nanocrystal spectroscopy must also provide an appropriate 2-level system. This last constraint can already be satisfied by most available nanocrystals as quantum confinement energies are many orders of magnitude greater than predicted coupling energies. This holds true even for the band-edge exciton fine structure. Furthermore, nanocrystal shape modification may provide further ways to modify the spectroscopy in order to provide a suitable 2-level system in other nanocrystals.[28]

One of the most stringent constraints on the nanocrystal system is the requirement for low decoherence of the excited state. In the solid-state environment, phonons are the main contributors to excited state decoherence. Optical phonons can easily be removed from the solid-state environment by cooling to temperatures below the optical phonon cut-off energy. However, acoustic phonons are widely dispersive and exist down to zero temperature. Nevertheless, nanocrystal materials are of sufficiently small size that the acoustic phonon band becomes discretized and it becomes possible to cool the system to a temperature below that which can excite the first acoustic phonon state in the nanocrystal. A temperature below 20 K is usually sufficient to freeze out all phonons in a nanocrystal. In a phonon-free environment, it is possible to obtain lifetime-limited linewidths.[29,30] Linewidths narrower than k_BT have already been observed in CdSe nanocrystals cooled to below 10 K,[31] and ensemble linewidths close to 1 GHz have been observed.[32] This is very promising for limiting exciton dephasing. Unfortunately, the lowest exciton level is often an optically forbidden transition, or dark state which causes additional dephasing and even exciton trapping in many different quantum dots. This obstacle does not seem to be present for the IV-VI lead chalcogenide nanocrystals, which is very promising.

Conclusion

We have investigated the use of the Stark tuning property of a nanocrystal quantum dot in order to control the quantum interaction with a high Q/V microcavity. A photonic CNOT gate based on the strong cavity coupling between both the excitonic and bi-excitonic transitions in a nanocrystal quantum dot and four non-degenerate field modes of a high Q/V fused silica microcavity was proposed. For this gate, the quantum dot is used only as a quantum bus that transfers and manipulates quantum information contained in the cavity modes. We have attempted to use realistic parameters in our model to obtain a reasonable estimate of what may be obtained experimentally. The manufacture of microcavities with sufficiently low loss and high Q/V ratio can be readily achieved with existing technology. Recent advances in nanocrystal fabrication have prompted us to consider the use of the bi-excitonic transition in nanocrystal quantum dots. Once we are well into the strong coupling regime, we find that initial state preparation can be accomplished with fidelities greater than 99

While the performance of this gate seems promising, it still requires further development in both microcavity fabrication as well as demonstration of appropriate nanocrystal properties, such as high resolution observation of the exciton and bi-exciton linewidths as well as the observation of vacuum Rabi splitting or vacuum Rabi oscillations. Further improvements to the gate protocol could involve using quantum interfernece to relax the contraint on the bi-exciton loss rate. Nevertheless, the model serves to highlight the possibility of using the dc Stark tunability of a nanocrystal quantum dot provides a useful means to control cavity QED interactions for potential quantum technologies.

REFERENCES

1. Knill E., Laflamme R., Milburn G. J., Nature **409**, 46 (2001).
2. O'Brien J. L., Pryde G. J., White A. G., Ralph T. C., Branning D., Nature **426**, 264 (2003).
3. Pittman T.B., Fitch M.J., Jacobs B.C., Franson J.D., Phys. Rev. A **68** (3) 032316 (2003).
4. Gasparoni S, Pan JW, Walther P, Rudolph T, Zeilinger A, Phys. Rev. Lett. **93** (2), 020504 (2004).
5. Nemoto K., Munro W. J., Phys. Rev. Lett. **93** (25), 250502, (2004).

6. Armani D. K., Kippenberg T. J., Spillane S. M., Vahala K. J., Nature **421** (6926), 925-928 (2003).
7. Spillane S. M., Kippenberg T. J., Vahala K. J., Goh K. W., Wilcut E., Kimble H. J., Phys. Rev. A **71** (1), 013817 (2005).
8. Song B.S., Noda S., Asano T., Akahane Y., Nat. Mat. **4** (3), 207 (2005).
9. Vernooy D. W., Furusawa A., Georgiades N. P., Ilchenko V. S., Kimble H. J., Phys. Rev. A **57** (4), R2293-R2296 (1998).
10. Buck J. R., Kimble H. J., Phys. Rev. A **67** (3), 033806 (2003).
11. McKeever J., Boca A., Boozer A. D., Miller R., Buck J. R., Kuzmich A., Kimble H. J., Science **303** (5666), 1992-1994 (2004).
12. Santori C., Fattal D., Vuckovic J., Solomon G., Yamamoto Y., Nature **419**, 594 (2002).
13. Santori C., Fattal D., Vuckovic J., Solomon G., Yamamoto Y., Fortschr. Phys. **52** (11-12), 1180 (2004).
14. Pelton M., Santori C., Vuckovic J., Zhang B. Y., Solomon G. S., Plant J., Yamamoto Y., Phys. Rev. Lett. **89** (23), 233602 (2002).
15. Kiraz A., Atature M., Imamoglu A., Phys. Rev. A **69** (3), 032305 (2004).
16. Kiraz A., Reese C., Gayral B., Zhang L., Schoenfeld W., Gerardot B., Petroff P., Hu E., Imamoglu A., J. Opt. B: Quantum Semiclass. Opt **5**, 129 (2003).
17. Li X.Q., Wu Y.W., Steel D., Gammon D., Stievater T.H., Katzer D.S., Park D., Piermarocchi C., Sham L.J., Science **301** (5634), 809-811 (2003).
18. Rauschenbeutel A., Nogues G., Osnaghi S., Beret P., Brune P., Raimond J., Haroche S., Phys. Rev. Lett. **83** (24), 5166 (1999).
19. Empedocles S. A., Bawendi M. G., Science **278**, 2114 (1997).
20. Chen G., Bonadeo N., Steel D., Gammon D., Katzer D., Park D., Sham L., Science **289**, 1906 (2000).
21. Kang, I.; Wise, F. W., J. Opt. Soc. Am B **14**, 1632 (1997).
22. Allan G., Delerue C., Phys. Rev. B **70**, 245321 (2004).
23. Andreev, A.; Lipovskii, A., Phys. Rev. B **59**, 15402 (1999).
24. Tudury, G.; Marquezini, L.; Ferreira, L.; Barbosa, L.; Cesar, C., Phys. Rev. B **62**, 7357 (2000).
25. Wehrenberg B., Wang C., Guyot-Sionnest P., J. Phys. Chem. B **106**, 10634 (2002).
26. Du H., Chen C., Krishnan R., Krauss T., Harbold J., Wise F., Thomas M., Silcox J., Nano Lett **2** (11), 1321 (2002).
27. Cai M., Painter O., Vahala K., Phys. Rev. Lett., **85** (1), 74 (2000).
28. Peng X.G., Manna L., Yang W.D., Wickham J., Scher E., Kadavanich A., Alivisatos A.P., Nature **404** (6773), 59 (2000); Hu J.T., Li L.S., Yang W.D., Manna L., Wang L.W., Alivisatos A.P., Science **292** (5524), 2060 (2001); Hu J.T., Wang L.W., Li L.S., Yang W.D., Alivisatos A.P., J. Phys. Chem. B **106** (10), 2447 (2002).
29. Kammerer C., Cassabois G., Voisin C., Perrin M., Delalande C., Roussignol Ph., Gerard J., Appl. Phys. Lett. **81**(15), 2737 (2002).
30. Bonadeo N., Erland J., Gammon D., Park D., Katzer D., Steel D., Science **282**, 1473 (1998).
31. Empedocles S. A., Norris D. J., Bawendi M. G., Phys. Rev. Lett. **77** (18), 3873 (1996).
32. Palinginis P., Tavenner S., Lonergan M., Wang H., Phys. Rev. B **67**, 201307(R) (2003).